Poulain Alexandre (Orcid ID: 0000-0002-0488-3993)

Diffusion of H_2S from anaerobic thiolated ligand biodegradation rapidly generated bioavailable mercury

Authors

Benjamin R. Stenzler[1], Rui Zhang[1], Jeremy D. Semrau[2], Alan A. DiSpirito[3], and Alexandre J. Poulain[1]*†

Affiliations

[1]Biology Department, University of Ottawa, 30 Marie Curie, Ottawa, ON K1N 6N5, Canada

[2]Department of Civil and Environmental Engineering, University of Michigan, Ann Arbor, MI 48109, USA.

[3]Roy J. Carver Department of Biochemistry, Biophysics and Molecular Biology, Iowa State University, Ames, IA 50011, USA

*Corresponding author. Email: apoulain@uottawa.ca

This is the author manuscript accepted for publication and has undergone full peer review but has not been through the copyediting, typesetting, pagination and proofreading process, which may lead to differences between this version and the Version of Record. Please cite this article as doi: 10.1111/1462-2920.16078

Summary

Methylmercury (MeHg) is a potent neurotoxin that biomagnifies through food webs and which production depends on anaerobic microbial uptake of inorganic mercury (Hg) species. One outstanding knowledge gap in understanding Hg methylation is the nature of bioavailable Hg species. It has become increasingly obvious that Hg bioavailability is spatially diverse and temporally dynamic but current models are built on single thiolated ligand systems, mostly omitting ligand exchanges and interactions, or the inclusion of dissolved gaseous phases. In this study, we used a whole-cell anaerobic biosensor to determine the role of a mixture of thiolated ligands on Hg bioavailability. Serendipitously, we discovered how the diffusion of trace amounts of exogenous biogenic H_2S, originating from anaerobic microbial ligand degradation, can alter Hg speciation - away from H_2S production site - to form bioavailable species. Regardless of its origins, H_2S stands as a mobile mediator of microbial Hg metabolism, connecting spatially separated microbial communities. At a larger scale, global planetary changes are expected to accelerate the production and mobilization of H_2S and Hg, possibly leading to increased production of the potent neurotoxin; this work provides mechanistic insights into the importance of co-managing biogeochemical cycle disruptions.

Originality-Significance Statement

This study demonstrates a mechanism in which microbes can liberate mercury from non-bioavailable thiol sinks through the generation and rapid diffusion of gaseous H_2S, making mercury immediately accessible to microbes in neighboring systems.

Keywords: mercury bioavailability, biosensors, sulfide, anoxic, diffusion

Introduction

Methylmercury (MeHg) is a neurotoxin of concern because it biomagnifies through food webs (Driscoll et al., 2013) and concentrates in food staples such as fish (Obrist et al., 2018) and rice (Tang et al., 2020). MeHg in the environment is produced by anaerobic microbes, particularly sulfate and iron-reducing bacteria, and methanogens (Podar et al., 2015). Methylation of divalent mercury (Hg(II)) is an intracellular process, and therefore Hg-bioavailability to microbes is a critical step (Regnell and Watras, 2019), which, in part, depends on Hg(II) speciation (i.e., the inorganic and organic ligands it is bound to) (Hsu-Kim et al., 2013; Regnell and Watras, 2019). Hg(II) has a high affinity for reduced sulfur (S) moieties ((e.g., $Hg(cysteine)_2$, $Hg(glutathione)_2$, HgS^0 or $Hg(HS)_2^0$). These Hg(II) species form with different substrates; low molecular weight thiols, microbial membranes, dissolved organic matter (DOM), and extracellular polymeric substances that form biofilms (Drott et al., 2013; Hsu-Kim et al., 2013; Manceau et al., 2015; Liem-Nguyen et al., 2017a; Liem-Nguyen et al., 2017b; Dranguet et al., 2018; Fein et al., 2019). These Hg(II)-thiol complexes do not uniquely define Hg bioavailability as some Hg(II) species are bioavailable to microbes while others are not (Schaefer et al., 2011; Zhao et al., 2017; An et al., 2019; Yin et al., 2020). Decoupling Hg(II) S-associated speciation from bioavailability in environments where Hg methylation occurs is necessary for modeling environmental constraints on Hg methylation.

The current model describing how Hg species enter microbial cells involves either an active transport of Hg thiol species and/or the passive diffusion of Hg(II)-sulfide complexes (Regnell and Watras, 2019). For Hg(II) species to enter the cell via non-specific metal ion transporters (Schaefer et al., 2011; Schaefer et al., 2014; Ndu et al., 2015; Szczuka et al., 2015), a ligand exchange must occur between the ligand in solution and the transport site on the cell

membrane (Schaefer et al., 2014; Thomas et al., 2014). Thiols can create labile Hg(II) species that can shuttle Hg to the transport site, but high concentrations of these thiols can also sequester Hg(II), preventing its transport across the cell wall (Schaefer and Morel, 2009; Schaefer et al., 2011; Ndu et al., 2012; Thomas et al., 2014; Lin et al., 2015; Liu et al., 2016; Zhao et al., 2017). Furthermore, any levels of multidentate thiol ligands such as sorption sites on microbial membranes, dissolved organic matter, and low molecular weight thiols bind Hg so strongly that they typically inhibit Hg(II) uptake (Hu et al., 2013a; Chiasson-Gould et al., 2014; Liu et al., 2016; Mishra et al., 2017; Song et al., 2018; Song et al., 2020; Thomas et al., 2020; Yin et al., 2020). Under most environmentally relevant conditions, inorganic sulfides will outcompete thiols for Hg(II) speciation and form Hg(II)-sulfide complexes (Deonarine and Hsu-Kim, 2009; Pham et al., 2014; Poulin et al., 2017) typically present as HgS nanoparticles that can be used as substrates for Hg methylation. Newly formed small Hg(II)-sulfides can permeate readily through cytoplasmic membranes (Zhou et al., 2017; Thomas et al., 2018; An et al., 2019; Thomas et al., 2019; Tian et al., 2021). However, given enough time and elevated Hg(II) concentrations, these HgS particles can aggregate and become too large and unavailable to cells (Graham et al., 2012, 2013; Mazrui et al., 2018; Zhang et al., 2020; Tian et al., 2021).

The areas of highest Hg methylation are not simple ligand systems, however. Methylation occurs in (micro)-anoxic zones of microbial ecosystems, such as biofilms or microbial mats (Olsen et al., 2016; Dranguet et al., 2018), the oxycline in water/sediments (Bravo et al., 2014), and in suspended particulate organic matter (Sunderland et al., 2009; Lehnherr et al., 2011; Ortiz et al., 2015). These environments are typically characterized by rapid nutrient turnover across redox gradients. This is the case for rapid and often cryptic sulfur cycling (Pester et al., 2012; Leclerc et al., 2015; Mills et al., 2016; Beulig et al., 2019; Jørgensen et al., 2019; Raven et al.,

2021), such as the transformation of high valences (S(VI); e.g., SO_4^{2-}) and low valence sulfur containing molecules (S(-II); e.g., thiols and H_2S). This process creates localized elevated µM-mM concentrations of thiols and transient H_2S production (Beulig et al., 2019; Jørgensen et al., 2019; Huynh et al., 2020; Raven et al., 2021). Extracellular thiols are generated by almost all forms of life (e.g., microbes, plants, algae, dissolved organic matter (DOM)) (Kawakami et al., 2006; Carrasco-Gil et al., 2011; Yu et al., 2014; Dunham-Cheatham et al., 2015; Mangal et al., 2016; Adediran et al., 2019), and H_2S is primarily produced by sulfur-reducing organisms (through dissimilatory SO_4^{2-} reduction pathways) (Labrenz et al., 2000; Pester et al., 2012; Mills et al., 2016; Jørgensen et al., 2019), but can also result from mineralization of organic molecules (Manceau et al., 2015; Enescu et al., 2016).

The role of thiolated ligands on Hg(II) bioavailability has received a lot of attention, and more recently, an effort has been made to further explore how microbial interactions can alter the fate of Hg(II). Most notably, the interactions between methanotrophic bacteria and Hg-methylating microbes have received much attention. Methanotrophs thrive at the oxic/anoxic interface and have also been shown to control Hg bioavailability to other organisms with production of the chalkophore, methanobactin (MB) (Semrau and Gu, 2020). While MB is secreted by methanotrophs to acquire copper, it has been shown to also interact strongly with Hg(II), altering bioavailability to both methanotrophs (Vorobev et al., 2013) and Hg-methylating microbes (Yin et al., 2020).

Whereas the study of individual ligands is essential to building conceptual models, we need to move away from single ligands to properly model Hg(II) bioavailability in complex microbial systems. Hg(II) speciation is dynamic, involves a series of ligand exchanges, and cannot be assumed to always be at equilibrium. To identify mechanisms underlying the dynamic

nature of Hg bioavailability in methylation sites, our lab has so far mostly focused on anaerobic Hg redox processes (Grégoire and Poulain, 2018; Branfireun et al., 2020) to evaluate whether these reactions can "reset" Hg speciation bound to otherwise poorly bioavailable ligands (e.g., multidentate thiols and DOM). Indeed, newly anaerobically produced Hg^0 may be reoxidized and become available for methylation (Colombo et al., 2013; Hu et al., 2013b) or diffuse away (evade) as a gas. Gases are not limited to the aqueous phase and are essential for Hg transport and cycling in the environment through evasion and deposition (Driscoll et al., 2013). This unique property of Hg emphasizes the importance of including (dissolved) gaseous phases at a scale that is relevant to microbial processes, and not only in global atmospheric models, when attempting to model Hg bioavailability to methylators.

In this study, we used a whole-cell anaerobic Hg-biosensor to determine the role of a mixture of thiolated ligands on Hg(II) bioavailability and serendipitously discovered a role for biogenic H_2S diffusion in controlling Hg(II) bioavailability at a distance. The Hg and sulfur cycles are intrinsically linked, but we have yet to consider the role of diffusive gaseous H_2S in controlling Hg(II) bioavailability. Here, we show how H_2S, either biogenic or added as Na_2S, diffuses away from the solution where it was produced, making an otherwise non-bioavailable Hg(II) species located at a distance rapidly available for microbial uptake.

Results and Discussion

Identifying bioavailable and non-bioavailable Hg(II) thiolated species

The first objective was to use a biosensor to determine which thiols, and at what concentrations, control anaerobic Hg(II) bioavailability. The addition of glutathione (GSH), methanobactin from *Methylosinus trichosporium* OB3b (MB-OB3b) and dimercaptosuccinic acid (DMSA) to the

exposure assay completely inhibited the fluorescence response of the Hg-inducible biosensor (μ=0) at 1 μM (0.026 RFU± 0.035, p = 0.131), 5 μM (-0.09 RFU ± 0.02, p = 0.002) and 0.1 μM (-0.003 RFU ± 0.095, p = 0.943) respectively (Fig. 1, A, B and C). The addition of these thiols did not inhibit constitutive fluorescence production by the biosensor, showing that a decrease in the inducible fluorescent signal was not associated with a reduction in cell viability under the conditions tested. In fact, the addition of both GSH and the MB from *Methylosinus trisporium* OB3b (MB-OB3b) enhanced the constitutive biosensor's fluorescence up to 1.75 ± 0.37x and 2.30 ± 0.20x that of the control, indicating a physiological benefit to the presence of these thiols (Fig. 1 A and B).

By contrast, the addition of penicillamine (Pen), cysteine (Cys), and dimercaprol (BAL) enhanced maximum fluorescence up to 5.13 ± 1.09x (Pen), 1.53 ± 0.60x (Cys), and 3.00 ± 0.70x (BAL) the control (Fig. 1 D, E, and F). As ligands concentrations increased, fluorescence eventually decreased but, interestingly, was never completely inhibited – as was observed for GSH, MB-OB3b, and DMSA - even when up to 4 mM of Pen or Cys was added (Fig. 1 D, and F). The constitutive biosensor fluorescence response suggests that reduction in Hg-inducible fluorescence may result from physiological stress to excess of these thiols.

Our results support that Hg(II) bioavailability is highly dependent on its speciation. We modeled Hg(II) speciation with and without a representative cell membrane (Fig. 2 and Fig. S1) with parameters inferred from (Song et al., 2020). In the absence of a membrane, Hg(II) forms two thiol coordinated complexes with GSH/Pen/Cys (>2:1 [RSH]:[Hg]) over the entire concentration gradients used in the assay (Fig, S1 A, D, and E). Initially, it appears that two thiol coordinated complexes ($Hg(RS)_2$) for GSH/Pen/Cys are highly bioavailable at low ligand concentration. As ligand concentration increases, bioavailability lowers for each of these thiols

and is completely inhibited by GSH. Hg(II) bioavailability is better explained by complexation with the membrane (Fig. 2). $Hg(GSH)_2$ is likely not bioavailable since it prevents Hg(II) from forming membrane complexes (Fig. 1 A; Fig. 2 A). Increasing Pen and Cys concentration initially enhances Hg(II) bioavailability which may be explained by the 1-3% Hg(Mem-RS)(RS) species at 50 μM (Fig. 1 D and E; Fig. 2 D and E). Further increasing concentration forms 100% $Hg(RS)_2$ species that are still bioavailable but much less. However, as described in the next section, we cannot merely assume that Hg(II) bioavailability with Cys is related to the formation of Hg(II)-Cys complexes.

These results are consistent with the dynamic effects of thiol concentration on Hg(II) bioavailability. Increasing thiol concentrations first enhances bioavailability before higher concentrations decrease it (Regnell and Watras, 2019).

Hg(II) bioavailability with MB-OB3b may also be explained by a lack of complexation with the cell membrane. MB-OB3b cannot compete for Hg(II) (Fig. 2 B) when modeled at equilibrium. However, MB-OB3b was allowed to equilibrate with Hg(II) before cells were added to the system. Without membrane thiols competing for Hg(II), changes in Hg(II) speciation with increasing MB-OB3b concentrations follow changes in bioavailability (Fig. 1 B and Fig. 2 C). Once bound to MB-OB3b, Hg(II) is not likely going to achieve thermodynamic equilibrium in an aqueous solution. Similar observations have been made in an attempt to displace Hg(II) and Au(III) from MB-OB3b and MB from Methylocystis strain SB2 with divalent copper (Cu(II)). Despite having orders of magnitude higher binding constants, in competitive assays, Cu(II) could not displace Hg(II) or Au(III) and even preferentially bound Hg(II) over Cu(II) (Baral et al., 2014; Kalidass et al., 2015). Thermodynamic modeling of aqueous chemical species is typically

limited to the assumption of equilibrium; however, sometimes systems cannot achieve equilibrium.

The Hg-MB-OB3b complex may be also be too large, and steric restrictions are preventing ligand exchange with the membrane. Active Hg(II) transport occurs across the inner membrane of a cell (Schaefer et al., 2011; Schaefer et al., 2014; Ndu et al., 2015; Szczuka et al., 2015). *Enterobacteriaceae* have general "unspecific" porins on the outer membrane with a strict cut-off limit on the sizes of molecules that can permeate (600 Da). This is a critical factor in designing antibiotics (Choi and Lee, 2019). MB-OB3b has a molecular weight (MW) of 1154.26 Da (1354.85 Da with Hg(II)). Porin exclusion may also be happening with $Hg(GSH)_2$. Two GSH molecules have a MW 614.63 Da (813.23 Da as ($Hg(GSH)_2$). If this is the reason $Hg(GSH)_2$ and Hg-MB-OB3b are not bioavailable, performing ligand exchanges to form smaller Hg(II) species may facilitate bioavailability. The other ligands used in this study form Hg(II) complexes with a MW <600 Da.

Lastly, there was a stark contrast in Hg(II) bioavailability with BAL and DMSA (Fig. 1 C and F). Although these synthetic molecules are not naturally occurring in the environment, the rationale for using BAL and DMSA in the experimental design was to identify Hg(II) species that would be entirely non-bioavailable to test the ligand exchange hypothesis. Any amount of BAL would completely alter Hg(II) speciation (Fig. 2 F; Fig. S1 F). Whereas no stability constants are available for DMSA, we assume, similar to BAL, that any concentration of DMSA (>[Hg(II)] alters speciation entirely. Hg(BAL) species are highly bioavailable, while HgDMSA species have no bioavailability at all. The only notable difference between the two molecules is that DMSA complexes are charged and hydrophilic, and BAL complexes are lipophilic and neutral (Bjørklund et al., 2019). This may be a factor differentiating their bioavailability by

passive diffusion of HgBAL. However, assessing the ability of non-naturally occurring ligands to facilitate Hg(II) bioavailability through passive diffusion is beyond the scope of this study.

It is important to note that the models may not fully represent our system's Hg(II) speciation. We used modeling parameters to generally infer how Hg(II) speciation affects its bioavailability. The exact concentrations of thiols on the *E. coli* cell membrane have not been measured. They might be higher or lower than anticipated; this would skew the model. The recommended concentrations of membrane thiols also had an error of 13%. In addition, the constants for Hg(Mem-RS)(Pen) and Hg(Mem-RS)(GSH) complexes have not been measured but inferred from cysteine. These species are likely are forming (Song et al., 2018; Song et al., 2020), but this is yet to be verified experimentally, using a combination of spectroscopic methods.

Thiol Ligand Exchanges and Hg Bioavailability

After identifying the bioavailability of Hg(II) species using single ligands, we proceeded to test how ligand exchange affect Hg bioavailability. Changing Hg(II) speciation from non-bioavailable to bioavailable (e.g., $Hg(GSH)_2 \rightarrow Hg(Pen)_2$) should enhance Hg(II) uptake. We modelled Hg(II) speciation with GSH or MB-OB3b (5μM) with increasing concentrations of Pen or Cys (Fig. S2). By adding 50 and 500 μM of competing ligand we will completely alter the speciation and form bioavailable species (e.g., $Hg(Pen)_2$ and $Hg(Cys)_2$). However, the addition of 50 or 500 μM Pen did not rescue Hg(II) bioavailability in the presence of 5μM GSH or MB-OB3b (Fig. 3 A) by forming $Hg(Pen)_2$. The constitutive biosensor data indicated that this was not the result of stress possibly induced by the presence of a combination of ligands. The same observation was made with a combination of Pen and MB-OB3b (Fig. 3 A). Altering the speciation to form bioavailable Hg(II) species did not enhance Hg(II) bioavailability. It is

possible that ligand exchange did not occur, possibly because of kinetic/modeling constraints, but this is consistent for Hg(II) not being able to be displaced from MB-OB3b (Baral et al., 2014; Kalidass et al., 2015). We did not observe a fluorescence signal developing over 10 hours (Fig. 3 A) or 20 hours when we let the experiment last longer (data not shown).

In sharp contrast to the addition of Pen, the addition of Cys had a profoundly different effect on Hg-inducible fluorescent induction (Fig. 3 B). This was surprising because Pen is only a methylated analog of Cys. The addition of 50 and 500 μM Cys vastly increased Hg-Inducible fluorescence in both the GSH and MB-OB3b treatments. Initially, we assumed that ligand exchange to form $Hg(Cys)_2$ species made Hg(II) bioavailable. However, the control wells containing no Cys and only Hg(II), GSH, or MB-OB3b (Fig. 3B circled in red) also exhibited a signal consistent with enhanced bioavailability. These concentrations made Hg(II) non-bioavailable (Fig. 1 A and B).

Cys and Pen are differentially metabolized by cells. Microbes exposed to Cys (typically >100 μM) can degrade it to H_2S, ammonia, and pyruvate (Thomas et al., 2018; Thomas et al., 2019). This process is not reported to happen with Pen due to the fact that it is methylated. Therefore, we speculated that the presence of H_2S resulting from cysteine degradation could change Hg(II) speciation in solution to form bioavailable Hg(II)-sulfides (Thomas et al., 2018; Thomas et al., 2019). It takes nM levels of H_2S (>[Hg(II)]) to change Hg(II) speciation and form aqueous Hg(II)-sulfides (e.g., $Hg(HS)_2$ and $Hg(HS)^-$) or facilitate the precipitation of metacinnabar (β-$HgS_{(s)}$) (Fig. 4). That is, our modeling shows that at equilibrium, almost any amount of H_2S will begin to facilitate the precipitation β-$HgS_{(s)}$ and form aqueous Hg(II)-sulfides when 2 nM Hg(II) is in the presence of 5 μM GSH/ MB-OB3b or 50 μM Cys (Fig. 4 A, B and C). With 500 μM Cys present, it requires a little more H_2S (50-500 nM) to begin forming

aqueous Hg(II) sulfides but will only precipitate β-$HgS_{(s)}$ between 100 nM to 50 μM H_2S (Fig. 4 D). These Hg(II)-sulfides are likely forming in solution, however it is unclear whether aqueous species, β-$HgS_{(s)}$, or a combination of the two, are bioavailable. The differential metabolism of Cys and Pen to H_2S by microbial cells may explain why Cys but not Pen could make Hg(II) bioavailable with GSH and MB-OB3b.

The really surprising result was that the 0 μM Cys treatments that also contained 5 μM GSH or MB-OB3b showed fluorescent induction for the Hg-inducible biosensor (Fig. 3 B circled in red) even though no Hg(II) should have been bioavailable at these concentrations (Fig. 1 A and B). These experiments were performed in 96-well microplates with lids, but such lids do not hermetically isolate wells from one another. This is notable since the treatments in each panel of Figure 3 were performed in the separate 96-well microplates (Fig. S3).

H_2S is unlikely to stay in solution, especially at a neutral pH in a shaking microplate. At a pH 7 (pH of exposure medium), sulfide is present as both 50% HS^- and 50% H_2S species in solution ($H_2S = HS^- + H^+$, pKa =7). While only the H_2S species can diffuse as a gas, proton transfer is fast, allowing H_2S to readily diffuse to reach equilibrium with its partial pressure above the solution (Balls and Liss, 1983; Schwarzenbach, 2002). The previous observations led us to test the hypothesis that biogenic H_2S diffusion away from its production well was responsible for the enhanced Hg bioavailability in wells located at a distance. The diffusion of $H_2S_{(g)}$ could remotely affect Hg(II) speciation to form bioavailable Hg(II)-sulfides.

The diffusion of gaseous H_2S makes Hg(II) bioavailable

To test this hypothesis, we first determined the kinetics behind $H_2S_{(g)}$ production and migration in the microplate to determine how much could reasonably affect Hg(II). We measured

H_2S, as total dissolved sulfide (operationally measured as S^{2-}), produced by the biosensor in the exposure medium when exposed to 500 µM Cys and Pen (Fig. 5 A and B). After 4 hours, we measured 62.69 ± 7.01 µM of H_2S with 500 µM Cys, but H_2S remained below the limit of detection with 500 µM Pen or without any added thiol. In addition, no H_2S was detected with the biosensor metabolizing 5 µM GSH, 5 µM MB-OB3B, 1 µM BAL, or 1 µM DMSA after 4 hours or when left overnight and metabolizing it for 24 hours (Table S2). If trace H_2S was generated from the metabolism of these thiols (below detection), it was insufficient to affect Hg(II) speciation and bioavailability. This data confirmed the differential metabolism of Pen and Cys to H_2S by *E. coli*.

H_2S dispersion in the microplate was fast. This was demonstrated by adding 50 or 500 µM Na_2S (in exposure medium buffered at pH=7) in one-quarter of the microplate wells (Fig. 5 C). For both 50 or 500 µM Na_2S treatments (Fig. 5 D and E), 74-80% of the H_2S evaded the Na_2S treated wells after 15 minutes and >95% after 30 minutes. Within 15 minutes, H_2S was detected in all of the non-treated wells. The non-treated wells contained 2.22 ± 0.35 and 19.88 ± 1.27 µM H_2S/well for microplates with 50 or 500 µM Na_2S, respectively. In the microplates containing 50 µM Na_2S, H_2S was below the limit of detection in the non-treated wells after 30 minutes or 1 hour microplates containing 500 µM Na_2S. For perspective, it took the biosensor about 3 hours (Fig. 3 A) to produce 50 µM of biogenic H_2S that would be undetectable in the non-treated wells after 30 minutes (Fig. 3 E). Although transient, this [H_2S] in the non-treated wells is predicted to be enough to alter Hg(II) speciation in the presence of GSH or MB-OB3b (Fig. 4 A and B).

We then tested whether Cys-induced biogenic production of $H_2S_{(g)}$ (Fig. 6 A) or H_2S amended as Na_2S (Fig. 6 B), could remotely alter Hg(II) speciation bound to refractory thiols in

isolated microplate wells not amended with either Cys or Na_2S (Fig. 4 A and B). When no H_2S (biogenic or amended as Na_2S) was present in the microplates, there was no fluorescent induction from the Hg-inducible biosensor with 5 μM GSH, 5 μM MB-OB3b, and 1 μM DMSA over 10 hours (Fig. 6 C).

In the presence of biogenic $H_2S_{(g)}$, every treatment produced a fluorescent response over 10 hours (Fig. 6 D). The onset of fluorescence induction in the presence of biogenic H_2S was also dependent on the nature of the thiolated ligand present. Significant induction ($\mu = 0$, $p < 0.05$) was observed after 2.5 minutes (first measurement time, 2.5 minute increments are not shown on graph) for the control and 5 μM GSH, 32.5 minutes for 5 μM MB-OB3b, and 77.5 minutes for 1 μM DMSA. The addition of 50 or 500 μM Na_2S led to faster induction than with biogenic $H_2S_{(g)}$ and also ligand-dependent (Fig. 6 E and F). At 50 μM Na_2S added, significant induction ($\mu = 0$, $p < 0.05$) began after 2.5 minutes for the control and 5 μM GSH, and after 5 minutes for 5 μM MB-OB3b and 1 μM DMSA. At 500 μM Na_2S added, significant induction ($\mu = 0$, $p < 0.05$) began after 2.5 minutes for the control, 5 μM GSH, and DMSA, and after 10 minutes for 5 μM MB-OB3b. We note that the induction from biogenic $H_2S_{(g)}$ was delayed, but more sustained than that from $H_2S_{(g)}$ amended as Na_2S; this is likely because cells need some time to metabolize Cys and will continue to produce H_2S long after all the pulse of $H_2S_{(g)}$ from Na_2S addition had dispersed out of solution. There is little lag between H_2S diffusion and a change in Hg bioavailability (2.5 – 10 min for H_2S from Na_2S amendments and 2.5 – 77.5 min for biogenic H_2S). This lag time appears to be ligand-specific, but we lack evidence to evaluate whether it is associated with the strength of Hg-ligand binding. Ligand selectivity may hinder the process of Hg ligand exchange (thiol to sulfide). The addition of any amount of H_2S will completely alter Hg(II) speciation in the control wells in addition to GSH, MB-OB3b, or DMSA.

The overlap in increasing Hg-inducible signal observed for all treatments over the first few hours (Fig. 6 D, E, and F) may reflect the fact that Hg(II) speciation is likely the same across all treatments with the addition of H_2S.

Hg(II) bioavailability is likely the result of changes in Hg(II) speciation with sulfide. The exchange from thiols/DOM with sulfide will initially form metacinnabar (β-HgS) but can form more ordered α-HgS over time or under ideal conditions (Manceau et al., 2015; Poulin et al., 2017; Thomas et al., 2018). This formation of β-HgS is rapid and supported by X-ray Absorption Spectroscopy studies that showed the detection of Hg(II)-sulfide nanoparticles within an hour (Manceau et al., 2015; Poulin et al., 2017; Thomas et al., 2018). However, in the presence of far excess ligand (e.g., 1 mM cysteine), only α-HgS will only form (Thomas et al., 2018).

Several studies have shown the central role of sulfide in Hg methylation (Graham et al., 2012, 2013; Zhou et al., 2017; Mazrui et al., 2018; Thomas et al., 2018; An et al., 2019; Thomas et al., 2019; Zhang et al., 2020; Tian et al., 2021). Most recently, Tian *et al.* described the importance of Hg(II)-sulfides as a major driver of MeHg production (Tian et al., 2021). They showed that the crystalline structure formed during the early stage of HgS mineralization binds very favorably to natural ligands (e.g., DOM, and GSH) or cell surfaces, and specifically to zinc transporters (ZnuA). This binding to the cell surface greatly enhanced Hg(II) methylation. The aging of HgS nanoparticles changed their crystal structures, but not their sizes, which decreased Hg(II) binding and methylation. *E. coli s*trains, and especially the K-12 strain we use in our study, express the same zinc transporter (ZnuA) that Tian *et al.* (2021) deployed (The UniProt, 2021), and we posit that a similar binding/uptake sequence was observed with the biosensor, suggesting a common process across microbial species. In our study, we observed the effect of

changing Hg(II) speciation from Hg(II)-thiols to Hg(II)-sulfides within a matter of seconds to minutes. The formation of β-HgS formation may be a facilitating Hg(II) bioavailability. However, it is also possible aqueous Hg(II)-sulfides are also entering the cell through either active or passive transport.

The objective of this study was to investigate the influence of thiol ligand exchanges on Hg(II) bioavailability. We used model ligands to gain a mechanistic understanding of this process. Serendipitously, we reveal the importance of biogenic production of H_2S from ligand degradation and of its diffusion on Hg(II) bioavailability. This study demonstrates the profound and rapid role H_2S has, even far from its production site, on Hg(II) bioavailability, regardless of Hg(II) original speciation.

Environmental Implications

This study demonstrates the importance of including dissolved gaseous phases to better understand microbial Hg transformations. Until now, redox reactions appeared to be the main catalysts to possibly reset Hg speciation at sites where methylation occurs (Grégoire and Poulain, 2018; Branfireun et al., 2020) – i.e., producing freshly bioavailable Hg from an otherwise refractory Hg pool. Here we show how the diffusion of another gas, $H_2S_{(g)}$, can play a comparable role in altering Hg(II) speciation and allowing microbes to access Hg(II). H_2S concentrations are normally buffered at equilibrium by ferruginous conditions that can deplete the concentration of H_2S to nM levels through the precipitation of iron(II)-sulfides (Shakeri Yekta et al., 2014) or through microbial metabolisms (Jørgensen et al., 2019). These buffers are not always present or entirely efficient where the slow abiotic oxidation of H_2S allows it to diffuse away from its production site. Thus, (micro)organisms producing H_2S may influence Hg(II) speciation in systems devoid of endogenous H_2S production, prompting us to reevaluate

the possible interplay between S and Hg cycling and the conditions governing its bioavailability. When a metal is bound to DOM or present as a sulfide mineral, it is generally assumed that microbes cannot access it. The transition between these two phases with transient $H_2S_{(g)}$ may play a critical role in allowing microbes to access metals that are often essential catalysts for anaerobic metabolisms.

Global planetary changes are expected to remobilize previously sequestered Hg into the environment and accelerate S cycling. The roughly 793 gigagrams (874,133 tons) of Hg accumulated in the arctic permafrosts for thousands of years is now being released through climate change (Schuster et al., 2018). Combined with novel sources of H_2S produced through progressive eutrophication of aquatic ecosystems (Hinckley et al., 2020) and the mass global emergence of oceanic dead zones (Diaz and Rosenberg, 2008), humans can facilitate new conditions for Hg methylation. Our mechanistic findings suggest that the bioavailability of both sequestered and remobilized Hg will be exacerbated with increased global H_2S production. This will lead to rapid degradation of aquatic habitat quality and the production of more MeHg, a potent neurotoxin affecting the health of humans and wildlife. Whenever possible, co-management of global biogeochemical cycles (here S and Hg) may offer a path to mitigate some of the consequences of these changes.

Experimental Procedures

Experimental Design

Our study uses an anaerobic microbial biosensor to assess Hg(II) bioavailability as described in (Hinz et al., 2022). The Hg-biosensor, *Escherichia coli* NEB5α, emits a quantifiable fluorescent signal when Hg(II) enters the cell. Our biosensor can detect trace levels of Hg(II) (2 nM used in

this study) to identify Hg(II) bioavailability mechanisms at environmentally relevant Hg(II) concentrations. To assess the bioavailability of Hg(II) species, we addded a ligand to an exposure medium containing Hg(II) to form a Hg(II)-ligand complex as determined by thermodynamic modeling. We then combine these fluorescent readings with a constitutive biosensor, which always produces a fluorescent signal independent of the presence of Hg(II). This constitutive biosensor lets us distinguish Hg(II) bioavailability from the biosensor's viability (i.e, if the ligand negatively affects the biosensor's viability, it would not produce any fluorescent signal and give us a false negative for Hg(II) bioavailability).

The biosensor in our study, *E.. coli* NEB5α, functions anaerobically using fumarate as the terminal electron acceptor. Ideally, we would use a Hg methylating microbe to assess bioavailability, but *E. coli* NEB5α serves the purpose of a metabolically versatile Hg reporter system. In addition, unlike most Hg methylating microbes, *E. coli* will not generate H_2S as a byproduct of its general metabolism in the absence of excess cysteine (Thomas et al., 2018) or reduce Hg(II) (Grégoire et al., 2018). Therefore, we can dissociate gaseous phases of Hg(II) and H_2S from exogenous sources. Furthermore, fumarate reduction is a metabolism common among Hg(II) methylating microbes (sulfate and iron-reducing bacteria) (Schaefer et al., 2011; Yu et al., 2013; Si et al., 2015) and relevant to reducing environments.

The purpose of this study was to address the hypothesis that Hg(II) bioavailability can be enhanced by ligand exchange. **1)** We first identified which Hg(II)-thiol species were bioavailable and which ones were not. **2)** To test the ligand exchange hypothesis, we equilibrated Hg(II) with thiols that inhibit Hg(II) bioavailability then added thiols that were identified as forming bioavailable Hg(II) species and assessed the biosensor's response in the presence of this mixture, supported by thermodynamic modeling of Hg(II) speciation at equilibrium and **3)** we determined

how H_2S controls Hg(II) bioavailability to the biosensor. We controlled for the diffusion of H_2S into isolated wells of a 96-well microplate containing non-bioavailable Hg(II) species.

Reagents and chemical preparation

Glutathione (GSH) was purchased from Fisher Scientific Acros Organics Dimercaptopropanol (BAL), Meso-2,3-DimercaptoSuccinic Acid (DMSA) and L-Penicillamine (Pen) were purchased from Alfa Aesar. L-cysteine-free (Cys) base was purchased from MP biomedicals. Methanobactin from *Methylosinus trichosporium* OB3b (MB-OB3b) was isolated and characterized as described in (Bandow et al., 2011). All solutions were prepared anaerobically and in Coy Vinyl Anaerobic chamber (98% N_2, 1.5% H_2), and solvents were $N_{2(g)}$ bubbled to make anaerobic. All thiols except DMSA and BAL were made in anaerobic Milli-Q water. DMSA and BAL were dissolved in anaerobic, 100 % ethanol. All solutions mentioned were stored at -20 °C.

Bacterial Strains and Growth

Biosensors growth and suspension assays were performed as described in (Hinz et al; 2022). The method was modified to use fumarate as a terminal electron acceptor instead of nitrate as in our previous studies (Stenzler et al., 2018). Two microbial biosensors based in *E. coli* NEB5α (DH5α derivative of K12 strain) were deployed; a Hg-Inducible (*E. coli* NEB5α harboring the pUC57merR-Pp plasmid) and a Constitutive biosensor (*E. coli* NEB5α harboring pUC19AH206-Pp plasmid). The expression of a flavin-based fluorescent protein on the plasmids are regulated by the transcriptional regulator of the *mer* operon (*merR*) or a constitutive promoter. All anaerobic manipulations of cell cultures were performed in a Coy Vinyl Anaerobic chamber (98% N_2, 1.5% H_2). Anaerobic growth was performed in anaerobic balch tubes.

For anaerobic growth for suspension assay, *E. coli* biosensors were grown at 37˚C and the plasmids were selected with 200 µg/ml ampicillin (unless otherwise stated), no antibiotic was used in the suspension assay. From -80°C cryostock, the biosensors were plated onto fumarate-GMM plates (SI: fumarate reduction plates for recipe) with 100 µg/ml ampicillin and grown anaerobically in anaerobic plate jars (this took a couple of days). A single colony was selected and grown in anaerobic GMM (SI: Growth Medium for recipe) overnight. The following day, cultures were transferred (20% inoculum) into fresh GMM and grown to an OD_{600} of 0.6. Cultures were resuspended twice in anaerobic exposure medium (SI: Exposure Medium for recipe) supplemented with 10 mM Na_2Fumarate (10,000 RCF for 90 seconds). The cells were ready for a 1/20 dilution into the biosensor suspension assay in exposure medium.

Determination of Biogenic H_2S

The biosensor was prepared as such for the biosensor exposure assay. Instead of performing a 1/20 dilution of the biosensor into the suspension assay, the biosensor was added to a crimped serum bottle with an exposure medium containing no added thiol (Control), 500 µM Pen, 500 µM Cys, 5 µM GSH, 5 µM MB-OB3b, 1 µM BAL, and 1 µM DMSA. The serum bottles were placed in a shaking incubator at 37°C. Every 30 minutes (Pen and Cys) or 1 hour (Control, GSH, MB-OB3B, BAL and DMSA), the 5 mL medium was withdrawn from the serum bottles, filtered through 0.2-micron filters, and the H_2S was operationally quantified as $[S^{2-}]$ (µM) but reported as $[H_2S]$ (µM). Serum bottles were used to limit the evasion of H_2S and get a more accurate quantification of H_2S production that could not be done in a microplate. H_2S was measured using the methylene blue protocol method (Hach protocol Method 8131, USEPA method 376.2, and Standard Method 4500-S2– D for wastewater).

Biosensor suspension assays

Suspension assays were performed inside a Coy Vinyl Anaerobic chamber (98% N_2, 1.5% H_2). Suspension assays were performed in exposure medium using 7 ml standard PTFE vials. Hg(II) was prepared as a 7.2 µM $HgSO_4$ stock in 0.2 M H_2SO_4. The concentration was determined using an MA-3000 Mercury Analyzer. Hg was diluted in exposure medium to a working concentration of 100 nM in PTFE vials before addition to the suspension assay. The added reagents (thiols) to be equilibrated with Hg(II) were added before Hg(II). Hg(II) was added to the exposure medium at a final concentration of 2 nM and set to equilibrate for 30 minutes. Biosensor cells (as prepared from "Bacterial Strains and Growth") were added last as a 1/20 dilution into the suspension assay. The suspension assay was transferred (200 µL) in triplicate from the PTFE vials to a 96 well microplate (Black, 96-Well Clear-Bottom Nonbinding Surface Microplates) and transferred to a Synergy HTX plate reader (present in the anaerobic chamber). All assays that contained Cys or sulfide were performed in their own 96 well microplate.

Non-bioavailable Hg(II) species were identified by increasing thiol concentrations until the fluorescence of the biosensors was inhibited. Each thiol concentration gradient was performed in a separate 96-well microplate. The Hg(II) species were then determined using thermodynamic modelling. In some instances, inhibition was not observed, and therefore, we increased concentrations well beyond physiologically relevant conditions (up to 4 mM). Dimercaptopropanol (BAL) and dimercaptosuccinic acid (DMSA) used in this study are not naturally occurring in the environment but contain extremely high affinities for Hg(II) and have found use in chelation therapy. They were investigated in this study as we anticipated they would completely inhibit Hg(II) bioavailability.

Several modifications were made to the assay were made to address ligand exchanges and the diffusion of H_2S. Hg(II) was pre-equilibrated with GSH/MB-OB3b before adding Pen/Cys when performing ligand exchanges. For assays that used biogenic H_2S; when performing 1/20 dilution of the biosensor into the suspension assay, it was also added to the exposure medium containing 500 μM Cys. The biosensor/Cys mixture was then added to wells A1-A12 and H1-H12 of the 96 well microplates (1 quarter of the wells) immediately before placing them into the plate reader. To generate added non-biogenic H_2S, Na_2S was diluted from a 200 mM stock to either 50 or 500 μM in exposure medium for added H_2S. Like biogenic H_2S, these were immediately added to 1 quarter of the wells before placing it into the plate reader.

Readings for fluorescence, luminescence, and OD_{600} were taken every 2.5 minutes for 10 hours at 37 ˚C. Shaking continuously between reads. Fluorescence was read for PpFbFp (Excitation: 440 nm, Emission: 500 nm**).** Hg-inducible and constitutive fluorescence were measured at 10 hours. Calculations were performed as described in (Stenzler et al., 2018). All values were then normalized to the no thiol treatment control (2 nM Hg(II)) at 10 hours for each biological replicate in the assay. Biological replicates here are independent cell cultures prepared from a single colony selected from fumarate reduction plates (See "Bacterial Strains and Growth").

Determination of H_2S migration in 96 well microplates

The 96 well microplate plate was divided into 4 sections (Fig. S4); Sulfide treatment (wells A1-A12 and H1-H12), Section 1 (Wells B1-B12 and C1-C12), Section 2 (Wells D1-D12 and E1-E12), and Section 3 (Wells F1-F12 and G1-G12). 200 uL of exposure medium were added to all the wells in Sections 1-3. This was done to obtain enough volume to perform sulfide analysis. Then a concentrated sulfide standard (200 mM Na_2S) was diluted in exposure medium (6 mL, to

avoid Na_2S altering the pH) to a concentration of 50 or 500 µM. These sulfide solutions were added to the sulfide treatment wells. A plate lid was immediately placed on the 96 well microplates and placed in the plate reader. The plate reader ran the biosensor protocol for 15, 30, and 60 minutes before sulfide concentrations in each section were measured. For 0 minutes, the 96 well microplates were not placed in the plate reader. Every measurement for each time point was measured in an independent experiment and performed in triplicate.

Once the experiment was completed, all four sections (4.8 mL per section) were quickly withdrawn and added to 15 mL polypropylene centrifuge tubes containing 5mL of zinc trap solution (1 mM zinc acetate, 1 mM nitrilotriacetic acid, and 5 mM NaOH). Sulfide was measured using the methylene blue protocol method (Hach protocol Method 8131, USEPA method 376.2, and Standard Method 4500-S2– D for wastewater). The results for the sulfide concentration (µM $[H_2S]$/well) for each section individually are reported in Figure S4 (A and B). The sulfide concentration between sections 1-3 appeared to be homogenous, and therefore the average of the three sections are reported in the results as "exposure wells." The limit of detection of H_2S per well to account for the 2.08x dilution required to perform the sulfide measurements was (0.34 µM $[H_2S]$]/well).

Thermodynamic Modelling

All thermodynamic modeling was performed using PHREEQC (Parkhurst, 2013). All equilibrium constants used for calculations can be found in Table S3. All modeling was performed at 25 ˚C, in exposure medium (pH 7), with 2 nM Hg(II). Lack of thermodynamic constants to correct for temperature would make modeling with Hg(II) not be representative of 37˚C in the biosensor assay. Constants for thiols were only obtained from (Liem-Nguyen et al., 2017b; Song et al., 2018; Song et al., 2020) for internal consistency. These studies improve on

the methodology to refine difficult to measure Hg(II)-thiol stability constants by combining liquid chromatography–inductively coupled plasma mass spectrometry, EXAFS spectroscopy measurements, and Density functional theory calculations. These studies also take into account ligand exchanges, single thiol coordinated complexes (Hg(II)-SR), and heterocomplexes (R^1S-Hg-SR^2). The single thiol coordinate complexes represented in the models include coordination with one N/O groups on the same thiol molecule (Song et al., 2018). The stability constants for heterocomplexes were determined to be at least 1.5 log units smaller than the average stability constant for the corresponding two thiol coordinated complexes ($Hg(SR)_2$)(Liem-Nguyen et al., 2017b). Values for Hg(II)-sulfide speciation and metacinnabar (β-HgS(s)) precipitation were obtained from (Drott et al., 2013).

Models were made to include thiol complexation of Hg(II) on a representative cell membrane. All values are reported in Table S3. While no specific thiol site concentrations are measured specifically for *E. coli* used in our study, much work has gone into identifying modeling parameters. Surface thiol concentrations have been determined in *Bacillus, Shewanella*, *Pseudomonas*, *Geobacter,* and *Desulfovirbio sp.* (Glazyrina et al., 2010; Yu et al., 2014; Mishra et al., 2017; Song et al., 2020; Thomas et al., 2020). Roughly 5% of the total membrane-bound thiols are close enough to form two thiol coordinate bonds with Hg(II) (Mishra et al., 2017). This coordination has been demonstrated in *E. coli* using X-ray absorption near edge structure (XANES) (Thomas et al., 2014). The total membrane thiol sites recommended for the model are ($Mem\text{-}RS_{tot}$ = 380 ± 50 μmol $g^{-1}C$) (Mishra et al., 2017). Based on the standard conversion from *E. coli* OD_{600} to cell number ($1OD_{600} = 8 \times 10^8$ cells/ml) and *E. coli* dry weight ($3x10^{-13}$g/Cell). Also, assuming 50% TOC factor for dry weight (Mishra et al., 2017). ($0.6OD_{600}$ x $8x\ 10^8$)cells/mL x ($3x10^{-13}$ g/Cell) (dry weight) x 0.5 (TOC content factor) x (380 μmol

thiols)/(gTOC) x 1/20 (dilution factor into assay) x 1000mL/L = 1.37 µM thiols in the assay. 5% (68nM) are capable of forming two thiol coordinated complexes ($Hg(Mem\text{-}RS)_2$) with other membrane functional groups ($Mem\text{-}R^{II}S^-$). All thiols were capable of forming two thiol coordinate complexes between the membrane and a ligand in solution (Hg(Mem-RS)(RS) or a single thiol coordinate complexes between a membrane thiol and a neighboring O/N functionality on the same molecule (Hg(Mem-RSRO). No thermodynamic data was available to form HgMem-RS(Pen)/HgMem-RS(GSH) complexes, and the values were inferred as Cys. These three low molecular weight thiols have similar stability constants with Hg(II) but vary over an order of magnitude ($Hg^{2+} + 2RS^- = Hg(RS)_2$, log k= 38.8, 37.5, 36.9 for GSH, Cys, Pen). While using only the constant for Cys will skew the model. Excluding them from the model will be less realistic since these species are likely to form (Song et al., 2018; Song et al., 2020).

Thermodynamic models were made to evaluate Hg(II) speciation over the gradient of thiols used in the biosensor assays. Models were made with and without the addition of thiols on the membrane. A mixture of $Hg(OH)_2$ and $Hg(NH_3)_x^{2+}$ species would form at 25˚C, but at 37˚C this would shift to ≈98% $Hg(OH)_2$. To simplify these models, $Hg(OH)_2$ and $Hg(NH_3)_x^{2+}$ species were displayed as $Hg(OH)_2$ only.

Thermodynamic models were made to demonstrate Hg(II) speciation shift by performing ligand exchanges. The first set of exchanges were with Cys and Pen to 5 µM MB-OB3b and GSH. Only GSH was modeled with a representative cell membrane. The second set of ligand exchange was with H_2S and only in systems that were determined to contain H_2S; 5 µM MB-OB3b, 5 µM GSH, 50 µM Cys, and 500 µM Cys. Interactions with the membrane were excluded from these models due to limited thermodynamic data between Hg(II)-sulfides and the membrane. Also, we modeled under the assumption that these species were not exchanging with

the membrane. There were no substantial changes (at most, 1%) in speciation distributions in systems with 50 μM and 500 μM Cys with the addition of 5 μM GSH/MB-OB3b, therefore only models of 50 μM Cys and 500 μM Cys are shown. We did not enable precipitation of β-HgS(s) in the models, but its formation is indicated by the Saturation Index (SI). When the saturation index is above 0, the mineral is above saturation and should precipitate.

Statistical Analyses

To assess if Hg(II) bioavailability was completely inhibited by any variable added to the exposure medium, the normalized fluorescence needed to be equal to or less than zero. A two-tailed, one-sample t-test on Normalized Fluorescence (%) was performed (H_0, $\mu = 0$, with a confidence interval of 95%). To determine the time of significant normalized fluorescent induction, normalized fluorescence needed greater than zero. A one-tailed, one-sample t-test on Normalized Fluorescence (%) was performed on every measured time point (2.5 min intervals) (H_0, $\mu = 0$, with a confidence interval of 95%). The time point was reported if every time point after was also significant. Changes in Hg-bioavailability relative to the control were determined with a two-tailed, one-sample t-test on Normalized Fluorescence (%) (H_0, $\mu = 1$, with a confidence interval of 95%). Statistical Analyses were performed in Microsoft Excel.

References

G.A. Adediran, V. Liem-Nguyen, Y. Song, J.K. Schaefer, U. Skyllberg, and E. Björn (2019) Microbial Biosynthesis of Thiol Compounds: Implications for Speciation, Cellular Uptake, and Methylation of Hg(II). *Environmental Science & Technology* **53**: 8187-8196.

J. An, L. Zhang, X. Lu, D.A. Pelletier, E.M. Pierce, A. Johs et al. (2019) Mercury Uptake by Desulfovibrio desulfuricans ND132: Passive or Active? *Environmental Science & Technology* **53**: 6264-6272.

P.W. Balls, and P.S. Liss (1983) Exchange of H2S between water and air. *Atmospheric Environment (1967)* **17**: 735-742.

N.L. Bandow, W.H. Gallagher, L. Behling, D.W. Choi, J.D. Semrau, S.C. Hartsel et al. (2011) Isolation of Methanobactin from the Spent Media of Methane-Oxidizing Bacteria. *MethEnzymol* **495**: 259-269.

B.S. Baral, N.L. Bandow, A. Vorobev, B.C. Freemeier, B.H. Bergman, T.J. Herdendorf et al. (2014) Mercury binding by methanobactin from Methylocystis strain SB2. *Journal of Inorganic Biochemistry* **141**: 161-169.

F. Beulig, H. Røy, S.E. McGlynn, and B.B. Jørgensen (2019) Cryptic CH4 cycling in the sulfate–methane transition of marine sediments apparently mediated by ANME-1 archaea. *The ISME Journal* **13**: 250-262.

G. Bjørklund, G. Crisponi, V.M. Nurchi, R. Cappai, A. Buha Djordjevic, and J. Aaseth (2019) A Review on Coordination Properties of Thiol-Containing Chelating Agents Towards Mercury, Cadmium, and Lead. *Molecules* **24**.

B.A. Branfireun, C. Cosio, A.J. Poulain, G. Riise, and A.G. Bravo (2020) Mercury cycling in freshwater systems - An updated conceptual model. *Science of The Total Environment* **745**: 140906.

A.G. Bravo, C. Cosio, D. Amouroux, J. Zopfi, P.-A. Chevalley, J.E. Spangenberg et al. (2014) Extremely elevated methyl mercury levels in water, sediment and organisms in a Romanian reservoir affected by release of mercury from a chlor-alkali plant. *Water Research* **49**: 391-405.

S. Carrasco-Gil, A. Alvarez-Fernández, J. Sobrino-Plata, R. Millán, R.O. Carpena-Ruiz, D.L. Leduc et al. (2011) Complexation of Hg with phytochelatins is important for plant Hg tolerance. *Plant Cell Environ* **34**: 778-791.

S.A. Chiasson-Gould, J.M. Blais, and A.J. Poulain (2014) Dissolved Organic Matter Kinetically Controls Mercury Bioavailability to Bacteria. *Environmental Science & Technology* **48**: 3153-3161.

U. Choi, and C.-R. Lee (2019) Distinct Roles of Outer Membrane Porins in Antibiotic Resistance and Membrane Integrity in Escherichia coli. *Frontiers in Microbiology* **10**.

M.J. Colombo, J. Ha, J.R. Reinfelder, T. Barkay, and N. Yee (2013) Anaerobic oxidation of Hg(0) and methylmercury formation by Desulfovibrio desulfuricans ND132. *Geochimica et Cosmochimica Acta* **112**: 166-177.

A. Deonarine, and H. Hsu-Kim (2009) Precipitation of Mercuric Sulfide Nanoparticles in NOM-Containing Water: Implications for the Natural Environment. *Environmental Science & Technology* **43**: 2368-2373.

R.J. Diaz, and R. Rosenberg (2008) Spreading Dead Zones and Consequences for Marine Ecosystems. *Science* **321**: 926.

P. Dranguet, V.I. Slaveykova, and S. Le Faucheur (2018) *Kinetics of mercury accumulation by freshwater biofilms*.

C.T. Driscoll, R.P. Mason, H.M. Chan, D.J. Jacob, and N. Pirrone (2013) Mercury as a global pollutant: sources, pathways, and effects. *Environmental science & technology* **47**: 4967-4983.

A. Drott, E. Bjorn, S. Bouchet, and U. Skyllberg (2013) Refining thermodynamic constants for mercury (II)-sulfides in equilibrium with metacinnabar at sub-micromolar aqueous sulfide concentrations. *Environmental science & technology* **47**: 4197-4203.

S. Dunham-Cheatham, B. Mishra, S. Myneni, and J.B. Fein (2015) The effect of natural organic matter on the adsorption of mercury to bacterial cells. *Geochimica et Cosmochimica Acta* **150**: 1-10.

M. Enescu, K.L. Nagy, and A. Manceau (2016) Nucleation of mercury sulfide by dealkylation. *Sci Rep* **6**: 39359.

J.B. Fein, Q. Yu, J. Nam, and N. Yee (2019) Bacterial cell envelope and extracellular sulfhydryl binding s: Their roles in metal binding and bioavailability. *Chemical Geology*.

J. Glazyrina, E.M. Materne, T. Dreher, D. Storm, S. Junne, T. Adams et al. (2010) High cell density cultivation and recombinant protein production with Escherichia coli in a rocking-motion-type bioreactor. *Microb Cell Fact* **9**: 42.

A.M. Graham, G.R. Aiken, and C.C. Gilmour (2012) Dissolved Organic Matter Enhances Microbial Mercury Methylation Under Sulfidic Conditions. *Environmental Science & Technology* **46**: 2715-2723.

A.M. Graham, G.R. Aiken, and C.C. Gilmour (2013) Effect of Dissolved Organic Matter Source and Character on Microbial Hg Methylation in Hg–S–DOM Solutions. *Environmental Science & Technology* **47**: 5746-5754.

D.S. Grégoire, and A.J. Poulain (2018) Shining light on recent advances in microbial mercury cycling. *FACETS* **3**: 858-879.

D.S. Grégoire, N.C. Lavoie, and A.J. Poulain (2018) Heliobacteria Reveal Fermentation As a Key Pathway for Mercury Reduction in Anoxic Environments. *Environmental Science & Technology* **52**: 4145-4153.

E.-L.S. Hinckley, J.T. Crawford, H. Fakhraei, and C.T. Driscoll (2020) A shift in sulfur-cycle manipulation from atmospheric emissions to agricultural additions. *Nature Geoscience* **13**: 597-604.

A.J. Hinz, B. Stenzler, A.J. Poulain, and A. Bose (2022) Golden Gate Assembly of Aerobic and Anaerobic Microbial Bioreporters. *Applied and Environmental Microbiology* **88**: e01485-01421.

H. Hsu-Kim, K.H. Kucharzyk, T. Zhang, and M.A. Deshusses (2013) Mechanisms regulating mercury bioavailability for methylating microorganisms in the aquatic environment: a critical review. *Environ Sci Technol* **47**: 2441-2456.

H. Hu, H. Lin, W. Zheng, B. Rao, X. Feng, L. Liang et al. (2013a) Mercury reduction and cell-surface adsorption by geobacter sulfurreducens PCA. *Environmental Science and Technology* **47**: 10922-10930.

H. Hu, H. Lin, W. Zheng, S.J. Tomanicek, A. Johs, X. Feng et al. (2013b) Oxidation and methylation of dissolved elemental mercury by anaerobic bacteria. *Nature Geoscience* **6**: 751-754.

K. Huynh, V. Liem-Nguyen, C. Feng, R. Lindberg, and E. Björn (2020) Quantification of total concentration of thiol functional groups in environmental samples by titration with monobromo(trimethylammonio)bimane and determination with tandem mass spectrometry. *Talanta* **218**: 121109.

B.B. Jørgensen, A.J. Findlay, and A. Pellerin (2019) The Biogeochemical Sulfur Cycle of Marine Sediments. *Frontiers in Microbiology* **10**.

B. Kalidass, M.F. Ul-Haque, B.S. Baral, A.A. DiSpirito, and J.D. Semrau (2015) Competition between metals for binding to methanobactin enables expression of soluble methane monooxygenase in the presence of copper. *Applied and environmental microbiology* **81**: 1024-1031.

S.K. Kawakami, M. Gledhill, and E.P. Achterberg (2006) Production of phytochelatins and glutathione by marine phytoplankton in response to metal stress 1. *Journal of phycology* **42**: 975-989.

M. Labrenz, G.K. Druschel, T. Thomsen-Ebert, B. Gilbert, S.A. Welch, K.M. Kemner et al. (2000) Formation of Sphalerite (ZnS) Deposits in Natural Biofilms of Sulfate-Reducing Bacteria. *Science* **290**: 1744.

O. Lahav, A. Sagiv, and E. Friedler (2006) A different approach for predicting H2S(g) emission rates in gravity sewers. *Water Research* **40**: 259-266.

M. Leclerc, D. Planas, and M. Amyot (2015) Relationship between Extracellular Low-Molecular-Weight Thiols and Mercury Species in Natural Lake Periphytic Biofilms. *Environ Sci Technol* **49**: 7709-7716.

I. Lehnherr, V.L. St. Louis, H. Hintelmann, and J.L. Kirk (2011) Methylation of inorganic mercury in polar marine waters. *Nature Geoscience* **4**: 298-302.

V. Liem-Nguyen, U. Skyllberg, and E. Björn (2017a) Thermodynamic Modeling of the Solubility and Chemical Speciation of Mercury and Methylmercury Driven by Organic Thiols and Micromolar Sulfide Concentrations in Boreal Wetland Soils. *Environmental Science & Technology* **51**: 3678-3686.

V. Liem-Nguyen, U. Skyllberg, K. Nam, and E. Björn (2017b) Thermodynamic stability of mercury(II) complexes formed with environmentally relevant low-molecular-mass thiols studied by competing ligand exchange and density functional theory. *Environmental Chemistry* **14**: 243-253.

H. Lin, X. Lu, L. Liang, and B. Gu (2015) Cysteine Inhibits Mercury Methylation by Geobacter sulfurreducens PCA Mutant ΔomcBESTZ. *Environmental Science & Technology Letters* **2**: 144-148.

Y.-R. Liu, X. Lu, L. Zhao, J. An, J.-Z. He, E.M. Pierce et al. (2016) Effects of Cellular Sorption on Mercury Bioavailability and Methylmercury Production by Desulfovibrio desulfuricans ND132. *Environmental Science & Technology* **50**: 13335-13341.

A. Manceau, C. Lemouchi, M. Enescu, A.-C. Gaillot, M. Lanson, V. Magnin et al. (2015) Formation of Mercury Sulfide from Hg(II)–Thiolate Complexes in Natural Organic Matter. *Environmental Science & Technology* **49**: 9787-9796.

V. Mangal, N.L. Stock, and C. Guéguen (2016) Molecular characterization of phytoplankton dissolved organic matter (DOM) and sulfur components using high resolution Orbitrap mass spectrometry. *Anal Bioanal Chem* **408**: 1891-1900.

Nashaat M. Mazrui, E. Seelen, C.K. King'ondu, S. Thota, J. Awino, J. Rouge et al. (2018) The precipitation, growth and stability of mercury sulfide nanoparticles formed in the presence of marine dissolved organic matter. *Environmental Science: Processes & Impacts* **20**: 642-656.

J.V. Mills, G. Antler, and A.V. Turchyn (2016) Geochemical evidence for cryptic sulfur cycling in salt marsh sediments. *Earth and Planetary Science Letters* **453**: 23-32.

B. Mishra, E. Shoenfelt, Q. Yu, N. Yee, J.B. Fein, and S.C.B. Myneni (2017) Stoichiometry of mercury-thiol complexes on bacterial cell envelopes. *Chemical Geology*.

U. Ndu, R.P. Mason, H. Zhang, S. Lin, and P.T. Visscher (2012) Effect of inorganic and organic ligands on the bioavailability of methylmercury as determined by using a mer-lux bioreporter. *Applied and Environmental Microbiology* **78**: 7276-7282.

U. Ndu, T. Barkay, R.P. Mason, A.T. Schartup, R. Al-Farawati, J. Liu, and J.R. Reinfelder (2015) The use of a mercury biosensor to evaluate the bioavailability of mercury-thiol complexes and mechanisms of mercury uptake in bacteria. *PLoS One* **10**: e0138333.

D. Obrist, J.L. Kirk, L. Zhang, E.M. Sunderland, M. Jiskra, and N.E. Selin (2018) A review of global environmental mercury processes in response to human and natural perturbations: Changes of emissions, climate, and land use. *Ambio* **47**: 116-140.

T.A. Olsen, C.C. Brandt, and S.C. Brooks (2016) Periphyton biofilms influence net methylmercury production in an industrially contaminated system. *Environmental Science & Technology* **50**: 10843-10850.

V.L. Ortiz, R.P. Mason, and J.E. Ward (2015) An examination of the factors influencing mercury and methylmercury particulate distributions, methylation and demethylation rates in laboratory-generated marine snow. *Mar Chem* **177**: 753-762.

D.L.a. Parkhurst (2013) *Description of input and examples for PHREEQC version 3--a computer program for speciation, batch-reaction, one-dimensional transport, and inverse geochemical calculations*: Reston, Virginia : U.S. Department of the Interior, U.S. Geological Survey, 2013.

M. Pester, K.-H. Knorr, M. Friedrich, M. Wagner, and A. Loy (2012) Sulfate-reducing microorganisms in wetlands – fameless actors in carbon cycling and climate change. *Frontiers in Microbiology* **3**.

A.L.-T. Pham, A. Morris, T. Zhang, J. Ticknor, C. Levard, and H. Hsu-Kim (2014) Precipitation of nanoscale mercuric sulfides in the presence of natural organic matter: Structural properties, aggregation, and biotransformation. *Geochimica et Cosmochimica Acta* **133**: 204-215.

M. Podar, C.C. Gilmour, C.C. Brandt, A. Soren, S.D. Brown, B.R. Crable et al. (2015) Global prevalence and distribution of genes and microorganisms involved in mercury methylation. *Science Advances* **1**: e1500675.

B.A. Poulin, C.A. Gerbig, C.S. Kim, J.P. Stegemeier, J.N. Ryan, and G.R. Aiken (2017) Effects of Sulfide Concentration and Dissolved Organic Matter Characteristics on the Structure of Nanocolloidal Metacinnabar. *Environmental Science & Technology* **51**: 13133-13142.

M.R. Raven, R.G. Keil, and S.M. Webb (2021) Microbial sulfate reduction and organic sulfur formation in sinking marine particles. *Science* **371**: 178.

O. Regnell, and C.J. Watras (2019) Microbial Mercury Methylation in Aquatic Environments: A Critical Review of Published Field and Laboratory Studies. *Environmental Science & Technology* **53**: 4-19.

J.K. Schaefer, and F.M.M. Morel (2009) High methylation rates of mercury bound to cysteine by Geobacter sulfurreducens. *Nature Geosci* **2**: 123-126.

J.K. Schaefer, A. Szczuka, and F.M.M. Morel (2014) Effect of Divalent Metals on Hg(II) Uptake and Methylation by Bacteria. *Environmental Science & Technology* **48**: 3007-3013.

J.K. Schaefer, S.S. Rocks, W. Zheng, L. Liang, B. Gu, and F.M.M. Morel (2011) Active transport, substrate specificity, and methylation of Hg(II) in anaerobic bacteria. *Proceedings of the National Academy of Sciences* **108**: 8714-8719.

P.F. Schuster, K.M. Schaefer, G.R. Aiken, R.C. Antweiler, J.F. Dewild, J.D. Gryziec et al. (2018) Permafrost Stores a Globally Significant Amount of Mercury. *Geophysical Research Letters* **45**: 1463-1471.

R.P. Schwarzenbach, Gschwend, P.M. and Imboden, D.M. (2002) Air–Water Exchange. In Environmental Organic Chemistry (eds R.P. Schwarzenbach, P.M. Gschwend and D.M. Imboden). https://doi.org/10.1002/0471649643.ch20.

J.D. Semrau, and B. Gu (2020) Final Technical Report: Methanotrophic-Mediated Methylmercury Transformation: Characterization of Products, Mechanism, and Environmental Significance. In: University of Michigan.

S. Shakeri Yekta, B.H. Svensson, A. Björn, and U. Skyllberg (2014) Thermodynamic modeling of iron and trace metal solubility and speciation under sulfidic and ferruginous conditions in full scale continuous stirred tank biogas reactors. *Applied Geochemistry* **47**: 61-73.

Y. Si, Y. Zou, X. Liu, X. Si, and J. Mao (2015) Mercury methylation coupled to iron reduction by dissimilatory iron-reducing bacteria. *Chemosphere* **122**: 206-212.

Y. Song, T. Jiang, V. Liem-Nguyen, T. Sparrman, E. Björn, and U. Skyllberg (2018) Thermodynamics of Hg(II) Bonding to Thiol Groups in Suwannee River Natural Organic Matter Resolved by Competitive Ligand Exchange, Hg LIII-Edge EXAFS and 1H NMR Spectroscopy. *Environmental Science & Technology* **52**: 8292-8301.

Y. Song, G.A. Adediran, T. Jiang, S. Hayama, E. Björn, and U. Skyllberg (2020) Toward an Internally Consistent Model for Hg(II) Chemical Speciation Calculations in Bacterium–Natural Organic Matter–Low Molecular Mass Thiol Systems. *Environmental Science & Technology* **54**: 8094-8103.

B. Stenzler, J. Gaudet, and A.J. Poulain (2018) An Anaerobic Biosensor Assay for the Detection of Mercury and Cadmium. *JoVE*: e58324.

E.M. Sunderland, D.P. Krabbenhoft, J.W. Moreau, S.A. Strode, and W.M. Landing (2009) Mercury sources, distribution, and bioavailability in the North Pacific Ocean: Insights from data and models. *Global Biogeochemical Cycles* **23**.

A. Szczuka, F.M.M. Morel, and J.K. Schaefer (2015) Effect of Thiols, Zinc, and Redox Conditions on Hg Uptake in Shewanella oneidensis. *Environmental Science and Technology* **49**: 7432-7438.

Z. Tang, F. Fan, S. Deng, and D. Wang (2020) Mercury in rice paddy fields and how does some agricultural activities affect the translocation and transformation of mercury - A critical review. *Ecotoxicology and Environmental Safety* **202**: 110950.

C. The UniProt (2021) UniProt: the universal protein knowledgebase in 2021. *Nucleic Acids Research* **49**: D480-D489.

S.A. Thomas, T. Tong, and J.-F. Gaillard (2014) Hg(ii) bacterial biouptake: the role of anthropogenic and biogenic ligands present in solution and spectroscopic evidence of ligand exchange reactions at the cell surface. *Metallomics* **6**: 2213-2222.

S.A. Thomas, B. Mishra, and S.C.B. Myneni (2020) Cellular Mercury Coordination Environment, and Not Cell Surface Ligands, Influence Bacterial Methylmercury Production. *Environmental Science & Technology* **54**: 3960-3968.

S.A. Thomas, K.E. Rodby, E.W. Roth, J. Wu, and J.F. Gaillard (2018) Spectroscopic and Microscopic Evidence of Biomediated HgS Species Formation from Hg(II)-Cysteine Complexes: Implications for Hg(II) Bioavailability. *Environ Sci Technol* **52**: 10030-10039.

S.A. Thomas, P. Catty, J.-L. Hazemann, I. Michaud-Soret, and J.-F. Gaillard (2019) The role of cysteine and sulfide in the interplay between microbial Hg(ii) uptake and sulfur metabolism†. *Metallomics* **11**: 1219-1229.

L. Tian, W. Guan, Y. Ji, X. He, W. Chen, P.J.J. Alvarez, and T. Zhang (2021) Microbial methylation potential of mercury sulfide particles dictated by surface structure. *Nature Geoscience* **14**: 409-416.

A. Vorobev, S. Jagadevan, S. Baral Bipin, A. DiSpirito Alan, C. Freemeier Brittani, H. Bergman Brandt et al. (2013) Detoxification of Mercury by Methanobactin from Methylosinus trichosporium OB3b. *Applied and Environmental Microbiology* **79**: 5918-5926.

X. Yin, L. Wang, L. Zhang, H. Chen, X. Liang, X. Lu et al. (2020) Synergistic Effects of a Chalkophore, Methanobactin, on Microbial Methylation of Mercury. *Applied and Environmental Microbiology* **86**: e00122-00120.

Q. Yu, J. Szymanowski, S.C.B. Myneni, and J.B. Fein (2014) Characterization of sulfhydryl sites within bacterial cell envelopes using selective site-blocking and potentiometric titrations. *Chemical Geology* **373**: 50-58.

R.-Q. Yu, J.R. Reinfelder, M.E. Hines, and T. Barkay (2013) Mercury Methylation by the Methanogen Methanospirillum hungatei. *Applied and Environmental Microbiology* **79**: 6325-6330.

Z. Zhang, R. Si, J. Lv, Y. Ji, W. Chen, W. Guan et al. (2020) Effects of Extracellular Polymeric Substances on the Formation and Methylation of Mercury Sulfide Nanoparticles. *Environmental Science & Technology* **54**: 8061-8071.

L. Zhao, H. Chen, X. Lu, H. Lin, G.A. Christensen, and E.M. Pierce (2017) Contrasting Effects of Dissolved Organic Matter on Mercury Methylation by Geobacter sulfurreducens PCA and Desulfovibrio desulfuricans ND132. **51**: 10468-10475.

J. Zhou, M.D. Smith, S.J. Cooper, X. Cheng, J.C. Smith, and J.M. Parks (2017) Modeling of the Passive Permeation of Mercury and Methylmercury Complexes Through a Bacterial Cytoplasmic Membrane. *Environmental Science & Technology* **51**: 10595-10604.

Acknowledgments

We would like to thank Mija Azdajic for providing technical assistance and other members of the Poulain Lab at the University of Ottawa for providing outstanding moral fiber.

Funding:

This work was funded by an NSERC discovery grant, an Early Researcher Award from the Province of Ontario, and an NSERC Accelerator Grant funding to AJP.

Author contributions:

A.J.P. supervised the project. B.R.S., and A.J.P. designed the research and methodologies. J.D.S., and A.A.D. provided methanobactin samples and, together with R.Z., contributed to the experimental design. B.R.S performed the experiments. R.Z calibrated the biosensor to function on fumarate reduction. B.R.S and A.J.P. performed analyses on the data. B.R.S and A.J.P wrote the paper with contributions from J.D.S., A.A.D.

Competing interests:

The authors declare that they have no known competing interests.

Data and materials availability: All data needed to evaluate the conclusions in the paper are present in the paper and/or the Supplementary Materials. Additional data related to this paper may be requested from the authors.

Figure Legends

Figure 1: Hg(II) bioavailability in the presence of various thiols. Average Normalized Fluorescence measured as relative fluorescence units (RFU) ± 1SD at 10 hours emitted the Hg-Inducible biosensor (*E. coli* NEB5α harboring the pUC57merR-Pp plasmid) and the Constitutive biosensor (*E. coli* NEB5α harboring pUC19AH206-Pp plasmid) with the addition of **A)** glutathione (0-5 μM) **B** methanobactin from *M trichosporium* OB3b (MB-OB3b) (0-5 μM), **C)** DMSA (0-4000 μM), **D)** penicillamine (0-4000 μM), **E)** cysteine (0-4000 μM) and **F)** BAL (0-1 μM). Fluorescence at 10 hours was normalized to the control (0 μM) at 10 hours for each biological replicate (between 3 and 11 biological replicates per point, see Table S1 for further details). [Hg] was set to 2 nM. The experiment was performed at 37 ˚C in an anaerobic exposure medium (pH 7).

Figure 2: Hg(II) species with the addition of various thiols at equilibrium with a cell membrane. Thermodynamic model predicting the Hg speciation (%) with the addition **A)** glutathione (0-10 μM) **B** methanobactin from *M trichosporium* OB3b (MB-OB3b) (0-10 μM), **C)** MB-OB3b (0-10 μM) when no membrane thiols were included in the model, **D)** penicillamine (0-4000 μM), **E)** cysteine (0 -4000 μM) and **F)** BAL (0-1 μM). The models performed at 25˚C. The model contains a representative cell membrane with 1.37 μM thiols. With the membrane, Hg(II) can form two-coordinate thiols bonds between two thiols on the membrane ($Hg(Mem\text{-}RS)_2$), a mixed two-coordinate thiol complex between the membrane and a thiol in solution (Hg(Mem-RS)(RS)), or a one-coordinate thiol complex on the membrane with neighboring O/N functionality (Hg(Mem-RSRO). Models were performed in anaerobic exposure medium (pH 7), and [Hg(II)] was set to 2 nM.

Figure 3: Thiol ligand exchanges affect Hg(II) speciation and bioavailability. Average Normalized Fluorescence measured as relative fluorescence units (RFU) ± 1SD at 10 hours by Hg-Inducible biosensor (*E. coli* NEB5α harboring the pUC57merR-Pp plasmid) and the Constitutive biosensor (*E. coli* NEB5α harboring pUC19AH206-Pp plasmid). Measurements were made with the addition of **A)** penicillamine (Pen) (0, 50, or 500 μM) or **B)** cysteine (Cys) (0, 50, or 500 μM), when Hg(II) had already been equilibrated with 5 μM glutathione (GSH) or 5 μM methanobactin from *Methylosinus trichosporium* OB3b (MB-OB3b). Red circles around Hg-Inducible fluorescence highlight unexpected results. Fluorescence at 10 hours was normalized to the control (0 μM) at 10 hours for each biological replicate (between 4-5 biological replicates per point, see Table S1 for further details). The experiments and models were performed in anaerobic exposure medium (pH 7), and [Hg(II)] was set to 2 nM. The experiments were performed at 37 ˚C. The 50, 500 μM Cys and Pen treatments without GSH or MB-OB3b are the same data as Fig. 1.

Figure 4: Hg(II) species with the addition of H_2S. Thermodynamic model predicting the Hg speciation (%) (left axis) with the addition H_2S (0-25 μM) to **A)** 5 μM glutathione (GSH) **B)** 5 μM methanobactin from *M trichosporium* OB3b (MB-OB3b), **C)** 50 μM Cysteine (Cys), and **D)** 500 μM Cysteine (Cys). The model did not include precipitation but shows a saturation index of metacinnabar (β-HgS (SI) (right axis). Models were performed in anaerobic exposure medium (pH 7) and [Hg(II)] was set to 2 nM. The models performed at 25˚C.

Figure 5: H_2S produced by *E. coli* and migration in the 96 well microplate. A) Hydrogen sulfide (H_2S) (μM) produced by the Hg-Inducible biosensor in the presence of either 500 μM cysteine (Cys) or penicillamine (Pen) in anaerobic serum bottles. **B)** The H_2S (μM) ± 1SD over time (hours) in the presence of either 500 μM Cys, 500 μM Pen, or no added thiol (Control). The experiment was performed at 37 ˚C in an anaerobic exposure medium (pH 7) in triplicate. **C)** H_2S migration in the 96 well microplate from Na_2S treated wells (50 or 500 μM Na_2S in exposure medium) to exposure wells containing exposure medium. Average H_2S concentration per well measured as ($[H_2S]$/well) (μM) ± 1SD in the Na_2S treated wells and exposure wells after 0, 15, 30, and 60 minutes in the microplate reader in plates containing either **D)** 500 or **E)** 50 μM Na_2S. Measurements for each time point were measured in triplicate (3 separate 96 well microplates). Values with concentrations below the detection limit for H_2S (0.34 μM $[H_2S]$/well) are reported as zero.

Figure 6: Diffusion of both biogenic and added H_2S affect Hg(II) bioavailability in the presence of refractory thiols. A) Biogenic H_2S was generated in the 96 well microplate by the Hg-inducible biosensor (*E. coli* NEB5α harboring the pUC57merR-Pp plasmid) in the presence 500 μM cysteine or **B)** added H_2S in the 96 well microplate was generated by the addition of Na_2S (50 or 500 μM) into exposure medium. Sulfide (H_2S) diffused out of the wells containing H_2S and into wells containing the refractory thiols glutathione (GSH), methanobactin from *M trichosporium* OB3b (MB-OB3b), DMSA, and the Control (CTRL) that had equilibrated with 2 nM Hg(II). ¼ of the wells in the plate were used to generate H_2S. Average Normalized Fluorescence measured as relative fluorescence units (RFU) ± SD over time (hours) from the Hg-Inducible biosensor with the addition of 5 μM GSH, 5 μM MB-OB3b, 1 μM DMSA or no thiol (Control). These experiments were performed when **C)** No H_2S, **D)** Biogenic H_2S, **E)** 50 μM H_2S or **F)** 500 μM H_2S came from ¼ of the plate wells. Fluorescence was normalized to the control (0 μM) at 10 hours for each biological replicate. (For **C**, n = 23 for the control, n = 12 for GSH, n = 13 for MB-OB3b and n = 7 for DMSA. For **D**, n= 12 for the control, n = 8 for GSH and MB-OB3b, and n = 4 for DMSA. For **E**, n= 8 for the control, GSH and MB-OB3b, and n = 4 for DMSA). [Hg] was set to 2 nM. The experiment was performed at 37 ˚C in an anaerobic exposure medium (pH 7).

Supporting Information

Supplementary Text: recipes for growth and exposure media

Figure S1: Hg(II) species with the addition of various thiols without membrane thiols.

Figure S2. Hg(II) species with thiol ligand exchanges.

Figure S3: Plate templates with ligand exchanges using Penicillamine (Pen) and Cysteine (Cys).

Figure S4: Sulfide Migration in the 96 well microplate experimental design and raw data.

Table S1: Raw data for Figure 1 (A, B, C, D, E, and F), and Figure 2 (A and B), including the number of biologic replicates (n).

Table S2: H_2S produced by *E. coli* with added thiols.

Table S3. Stability constants ($\log_{10}K$) for all aqueous Hg(II)-species considered in the speciation calculations.

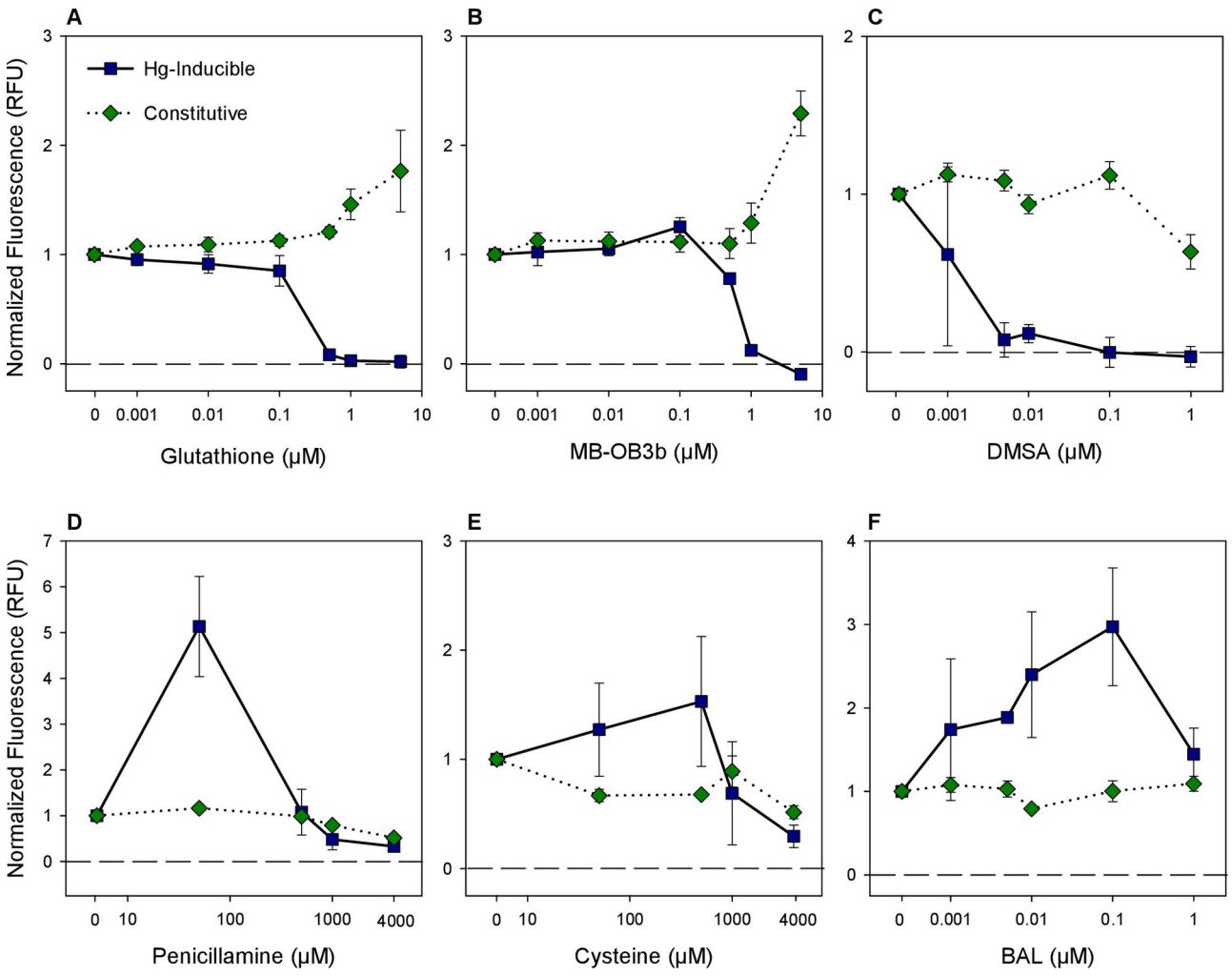

figure 1.EPS

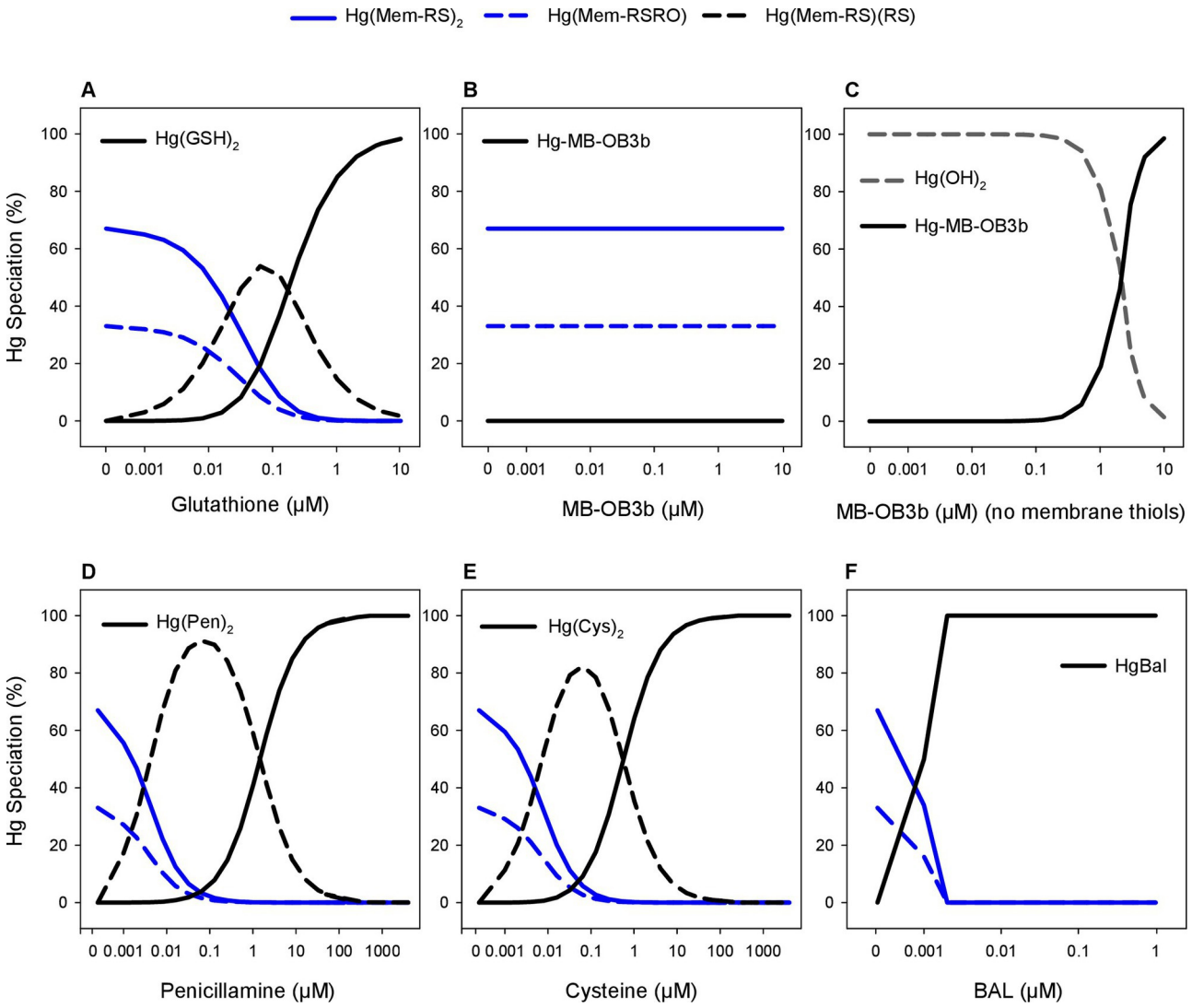

figure 2.EPS